Proc. Natl. Acad. Sci. USA
Vol. 92, pp. 9308–9312, September 1995
Cell Biology

The crystal structure of *Pseudomonas aeruginosa* exotoxin domain III with nicotinamide and AMP: Conformational differences with the intact exotoxin

MI LI*, FRED DYDA*, ITAI BENHAR†, IRA PASTAN†, AND DAVID R. DAVIES*‡

*Laboratory of Molecular Biology, National Institute of Diabetes and Digestive and Kidney Diseases, and †Laboratory of Molecular Biology, Division of Cancer Biology, Diagnosis and Centers, National Institutes of Health, Bethesda, MD 20892-0560

Contributed by David R. Davies, May 10, 1995

ABSTRACT **Domain III of *Pseudomonas aeruginosa* exotoxin A catalyses the transfer of ADP-ribose from NAD to a modified histidine residue of elongation factor 2 in eukaryotic cells, thus inactivating elongation factor 2. This domain III is inactive in the intact toxin but is active in the isolated form. We report here the 2.5-Å crystal structure of this isolated domain crystallized in the presence of NAD and compare it with the corresponding structure in the intact *Pseudomonas aeruginosa* exotoxin A. We observe a significant conformational difference in the active site region from Arg-458 to Asp-463. Contacts with part of domain II in the intact toxin prevent the adoption of the isolated domain conformation and provide a structural explanation for the observed inactivity. Additional electron density in the active site region corresponds to separate AMP and nicotinamide and indicates that the NAD has been hydrolyzed. The structure has been compared with the catalytic domain of the diphtheria toxin, which was crystallized with ApUp.**

Pseudomonas exotoxin A (PE) is a 66-kDa, 613-amino acid protein that is secreted by the bacterium *Pseudomonas aeruginosa* as one of its virulence factors (1, 2). The toxin binds to eukaryotic cells via the ubiquitous α_2-macroglobulin receptor (3), and enters the cells by receptor-mediated endocytosis. Once in the cells, the toxin is cleaved by a specific protease and, after reduction of a disulfide bond (4), a C-terminal fragment (aa 280–613) is released and subsequently translocated to the cytosol, where it catalyzes the irreversible inactivation of eukaryotic elongation factor 2 (eEF-2) by ADP-ribosylation of a modified histidine (diphthamide) residue, leading to the arrest of protein synthesis and eventually to cell death (1, 5). The crystallographic determination of the PE structure has shown that PE is made up of three domains (6) and that there is a correspondence between the structural and the functional boundaries of the domains. Domain Ia (aa 1–252) is responsible for cell recognition. Removal of domain Ia or a specific point mutation at position 57 results in an inactive toxin due to its inability to bind to cells (7). Domain II (aa 253–364) is involved in the translocation of the toxin across intracellular membranes. The function of domain Ib (residues 365–399) has not been elucidated. Removal of part of domain Ib (aa 365–380) results in a truncated but fully functional toxin (8). Domain III (aa 400–613) catalyzes the ADP-ribosylation of eEF-2 with the five C-terminal residues (REDLK) serving as an endoplasmic reticulum retention signal (9, 10). The functional boundary between domain Ib and domain III is located at residue 400 (8).

The ADP-transfer reaction catalyzed by domain III has been proposed to include formation of a binary complex of NAD and PE, binding of eEF-2 to the binary complex, and transfer of the ADP-ribose moiety of NAD to the diphthamide of eEF-2 as follows (11):

$$NAD^+ + \text{eEF-2} \overset{PE}{\rightleftharpoons} \text{ADP-ribose-eEF-2} + \text{nicotinamide} + H^+.$$

In the absence of eEF-2, a weak NAD-glycohydrolase activity can be detected:

$$NAD^+ + H_2O \overset{PE}{\rightleftharpoons} \text{ADP-ribose} + \text{nicotinamide} + H^+.$$

The mechanisms of these reactions have been investigated by crystallography and by site-directed mutagenesis (12–15), which has also been used to identify the region of NAD binding. Two active forms of PE are widely used in research. Activated PE can be obtained by treating PE with denaturing and reducing agents (16). Also, active fragments consisting of domain III and the C terminus of domains II and Ib (aa 280–613) have been produced by recombinant techniques or by enzymatic cleavage (5, 8, 16, 17). These fragments exhibit the same ADP-ribose-transferring activity but a stronger NAD-glycohydrolase reaction (17). Unlike the whole PE molecule, the toxin fragments or recombinant isolated domain III of PE (PEIII) do not require activation by urea and dithiothreitol to exhibit ADP-ribose transfer or NAD-glycohydrolase activities (ref. 16; unpublished data). Thus, it is likely that PEIII folds into a conformation resembling the one that is adopted *in vivo* by the enzymatically active C-terminal fragment which acts in the cell cytosol to inactivate eEF-2. Recombinant forms of PE containing domains II and III have been used as fusion proteins coupled to various forms of tumor-specific antibodies or to cytokines for targeted cytotoxicity (2, 18, 19).

Several other toxins with ADP-ribosyltransferase activity have been investigated by x-ray crystallography: cholera-toxin-related heat-labile enterotoxin (LT) (20), diphtheria toxin (DT) (21), and pertussis toxin (PT) (22). The enzymatic domain of all these display a folding pattern similar to PE. The similarity is even more striking around the active site—e.g., 44 residues from LT can be superimposed on the corresponding 44 residues from PE with a rms deviation of only 1.5 Å in C^α positions (22). Despite this structural similarity, however, there is no significant amino acid sequence identity between the two molecules. The recently reported crystal structure of the isolated catalytic domain of DT complexed with ApUp shows it to be essentially identical to the structure of the same domain in the intact DT (23).

The previous structural information on PE has come from the proenzyme form of the toxin in which the catalytic domain is inactive. However, to fully understand the mechanism of the ADP-ribose-transferring reaction, it is important to know the conformation of the active form of PE, especially the cleft area,

The publication costs of this article were defrayed in part by page charge payment. This article must therefore be hereby marked "*advertisement*" in accordance with 18 U.S.C. §1734 solely to indicate this fact.

Abbreviations: PE, *Pseudomonas* exotoxin A; PEIII, isolated domain III of PE; DT, diphtheria toxin; eEF-2, eukaryotic elongation factor 2.

‡To whom reprint requests should be addressed.

Table 1. Statistics of data collection, structure determination, and refinement

Resolution limit, Å	Observed reflections	Unique reflections	Shell completeness, %
5.00	12,374	2,393	95.0
4.00	11,786	2,161	96.4
3.50	11,463	2,148	96.5
3.15	12,108	2,366	94.6
2.90	10,718	2,286	88.5
2.70	9,918	2,351	83.9
2.60	4,951	1,320	77.3
2.50	5,021	1,488	73.9
Total reflections [2σ (I) cutoff]:		16,513	
R_{merge} (intensity)			0.068
Accumulated completeness, %			88.9
Refinement (8–2.5 Å, 2σ data)			
Free R factor			0.264
R factor			0.195
rms Δ bond length, Å			0.019
rms Δ bond angle, °			2.38
Protein atoms			3003
AMP and nicotinamide atoms			40
Water atoms			33

and how it interacts with the substrates. Here, we report the crystal structure of PEIII cocrystallized with NAD, describe the location of the nicotinamide and AMP portion of NAD in this domain, compare its conformation with that of domain III in PE and with the catalytic domain in DT, and discuss the NAD binding and structural basis of the ADP-transferring activity.§

EXPERIMENTAL PROCEDURES

PEIII was recovered from isopropyl β-D-thiogalactoside (IPTG)-induced cultures of *Escherichia coli* BL21(λE3) (24) carrying plasmid pPEΔ5-399. This plasmid, which encodes amino acids 1–4 followed by 400–613 of PE, preceded by an N-terminal methionine, is a derivative of pVC45f+T (7, 25) from which the DNA sequence encoding domains Ia, II, and Ib of PE was deleted by site-specific mutagenesis. The expressed protein accumulated in the periplasm and was recovered by sequential ion-exchange and gel-filtration chromatography essentially as described for whole PE (25). The hanging-drop vapor-diffusion method was used in a sparse matrix screen experiment to obtain initial conditions for crystallization (26). Microcrystals were grown for 3 days at room temperature under the following conditions. The well solution consisted of 800 μl of 1.5 M sodium citrate/40 mM NAD, pH 7.5. The 4-μl drop contained 2 μl of a solution of 10 mg of PEIII per ml of 10 mM Tris·HCl, pH 7.0/0.1 M NaCl mixed with 2 μl of the well solution. Crystals suitable for data collection were obtained by macroseeding. The crystal lattice was tetragonal with cell parameters a = 87.51 Å, c = 134.08 Å. The space group is $P4_32_12$, with two molecules per asymmetric unit. Diffraction data were collected using an R-AXIS-IIC imaging plate detector at room temperature and were processed with the R-AXIS software package. The data set used in structure determination and refinement contained 16,513 unique reflections (Table 1) greater than $2\sigma(I)$ which was 88.9% of the total possible reflections to 2.5-Å resolution.

Molecular Replacement. The crystal structure of PEIII was solved by molecular replacement, using the coordinates of domain III from the full-length toxin determined at 2.7-Å resolution (David McKay, personal communication). Both main and side chains were used in the search. The B factor for each atom was set to 15.0. The cross-rotation, translation, and rigid body optimization calculations were carried out with the AMORE package (27). In the cross-rotation search, reflections between 15 and 4.0 Å were used with an outer radius of 30 Å. All peaks greater than 50% of the maximum of the rotation function value were used in the translation search. The top 10 peaks greater than 50% of the maximum translation function were rigid body optimized. Two peaks corresponding to two different monomer solutions gave the highest correlation coefficient (0.462) and lowest R factor (42.3%). The dimer obtained from the above calculations satisfied the packing constraints imposed by the space group symmetry.

The model was refined by using X-PLOR with intensities $\geq 2\sigma$. First, a rigid body refinement was carried out in three stages. At the final stage, 8.5-Å to 3.0-Å resolution data were used, and the R factor decreased to 39.6%. This structure was then refined by simulated annealing, reducing the R factor to 25.7%. The resulting model was displayed with the graphics program O (28), verified, and rebuilt where necessary based on 2Fo − Fc and Fo − Fc electron density maps. Several segments in the original model were removed because of the poor density. They are 458–463 in monomer 1 and 579–580 in monomer 2. The main chains of 548–551 and 483–491, which were not defined in the original model, were built into the difference density in monomer 1. Some residues in the omitted regions were gradually incorporated into the structure. Density was observed between Tyr-481 and Tyr-470 in both monomers that could be fit well by the nicotinamide rings. AMP could be fitted to the density in the vicinity of residues 452–456 in monomer 2 (Fig. 1). Finally, the 33 waters with difference density greater than 3σ in the final Fo − Fc map were added. The results are summarized in Table 1.

RESULTS

The principal differences between PEIII and PE occur in the vicinity of the active site (Fig. 2). The crystal structure of the intact PE revealed an active-site cleft in domain III starting from the helix at aa 523–531 and ending at the helix at aa 445–453, with the loop at aa 454–468 on the top and residues 481, 440, and 553 on the bottom (6). The rms difference in C^{α} positions in the aa 458–463 loop between monomer 2 and PE is 7.6 Å, compared with an overall rms difference of 1.7 Å for

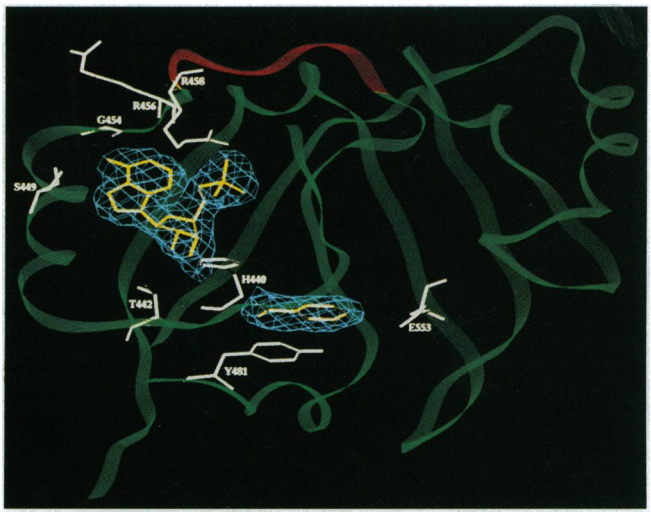

FIG. 1. (Fo − Fc) density in the active-site region of monomer 2. The final model of the AMP and nicotinamide are shown in yellow. The active-site loop (aa 458–463) is red. Side chains of residues involved in binding are shown in white.

§The atomic coordinates and structure factors have been deposited in the Protein Data Bank, Chemistry Department, Brookhaven National Laboratory, Upton, NY 11993 (reference IDMA).

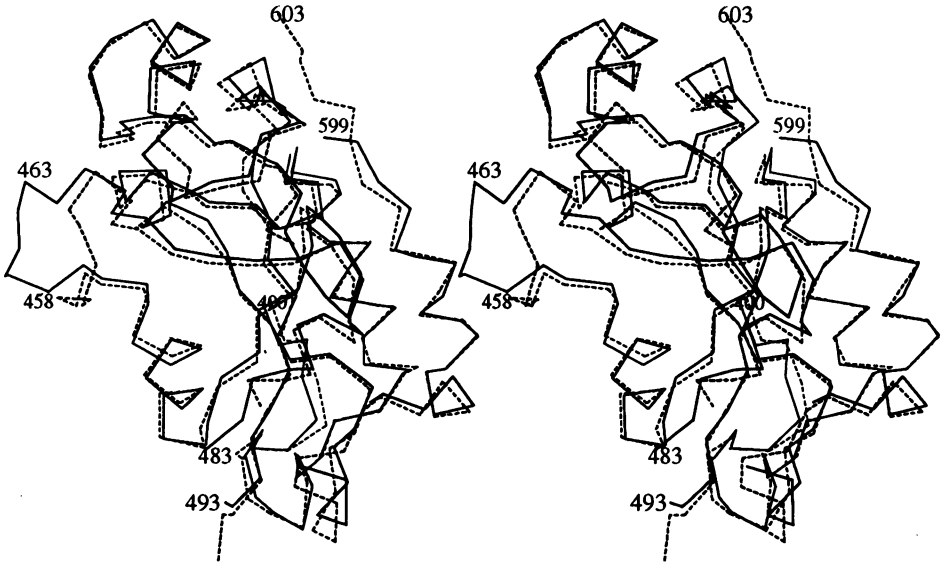

FIG. 2. Superposition of the isolated domain III of intact PE (dashed) on monomer 2 of PEIII (solid lines). The figure was drawn by using MOLSCRIPT (29).

all C^{α}s and 1.0 Å if this loop is omitted. As a result of this different conformation, the active-site cleft in monomer 2 is more open than in PE. In monomer 1, this loop is disordered and not part of the current model. Two loops not observed in the PE structure can now be defined in the PEIII structure. They are Gln-483 to Arg-491, and Glu-548 to Glu-551 in monomer 1. There is density at the C terminus of monomer 1 which permits the chain to be extended from Gln-603 to Arg-609. Some loop areas that were observed in PE are exposed to solvent in PEIII and could not be defined (Table 2). The aa 484–492 and aa 579–581 regions in monomer 2 are disordered. They correspond to the aa 68–74 and aa 173–175 regions in DT that were recently observed to undergo conformational change during the removal of the adjacent domain (23), which these authors propose as the first step in the activation of the catalytic domain.

Although NAD was included in the crystallization solution, it could not be seen intact in the electron density map, presumably because of the observed NAD-hydrolase activity of the enzyme (16). Density is found in both monomers that corresponds to nicotinamide, and in monomer 2, density corresponding to AMP was also observed (Fig. 1).

The nicotinamide can be fitted to the density in both monomers in two orientations: in one, the nicotine ring points toward Glu-553, and in the other, the amide points in this direction. Since Glu-553 has been implicated in the catalytic mechanism (12, 13), the first orientation is favored, although from the density alone, the second orientation could not be ruled out. The hydrogen-bond interactions with the protein also favor the first orientation, where the O and N atoms of the amide group form H bonds with main chain N and O atoms, respectively, of Gly-441 (2.70 Å and 2.83 Å in monomer 1 and 2.66 Å and 3.10 Å in monomer 2). In the second orientation, the H bonds between PEIII and nicotinamide are not formed, but close contacts are observed between C6 of the nicotine ring and the oxygen of Gly-441 (2.7 Å). In both cases, there are stacking interactions between the nicotinamide and the phenol ring of Tyr-481, with a separation of 3.56 Å in monomer 1 and 3.48 Å in monomer 2. Tyr-470 is located adjacent to the nicotinamide, but the orientation and distance between the two do not suggest that they interact through H bonds or by stacking.

The interactions between AMP and monomer 2 of PEIII are more complicated than those between nicotinamide and PEIII (Fig. 1; Table 3). They include H bonds, salt bridges, and stacking forces. The side chain of Arg-609 of a symmetry-related molecule also interacts with the adenine ring system, probably through stacking, and with the ribose and phosphate groups through H bonding (Table 3). The adenine also forms H bonds with Thr-449, Arg-456, and Gly-454. The ribose is H bonded to His-440 and Thr-442, and the phosphate oxygens are H bonded to the side chain of Arg-458 of monomer 2 and to Arg-609 from the symmetry-related monomer 1.

Table 2. Differences between PEIII and PE

Monomer 1 of PEIII	Monomer 2 of PEIII	PE
	Disordered regions	
458–463, 610–613	484–492, 579–580	483–491, 548–551
Side chain of 486	600–613	604–613
	Side chains of 546–548	
	Side chain of Arg-456, Gln-460	
	Side chain of Arg-551	
	Ligand binding	
Nicotinamide	AMP and nicotinamide	
	Conformational change in PEIII	
	458–463 in monomer 2	

DISCUSSION

Comparison of the Catalytic-Domain Structures of Intact PE and Monomer 2. The major difference between the struc-

Table 3. Interactions between AMP portion of NAD in PEIII and between adenine of ApUp and DT

Protein	Atoms	Distance, Å
PEIII	Ser-449 O^{γ} and N6A of adenine	2.61
	Arg-456 N and N1A of adenine	3.09
	Gly-454 O and N6A of adenine	3.25
	His-440 $N^{\epsilon 2}$ and O2′A of ribose	2.71
	Thr-442 $O^{\gamma 2}$ and O2′A of ribose	2.89
	Arg-458 $N^{\eta 1}$ and O2PA of phosphate	2.86
	Arg-609 $N^{\eta 2}$ and O5′A of ribose	2.64
	Arg-609 $N^{\eta 1}$ and O5′A of ribose	3.05
	Arg-609 $N^{\eta 1}$ and O2PA of phosphate	3.55
DT	Gln-36 N and N1A of adenine	3.03
	Gln-36 O and N1A of adenine	3.26
	Gly-34 O and N6A of adenine	3.20
	His-21 $N^{\epsilon 2}$ and O2′A of ribose	2.73

tures of the catalytic domain of the intact PE and the isolated PEIII is the new conformation of the loop at aa 458–463 observed in monomer 2. If monomer 2 of PEIII is superimposed upon domain III of PE, there are many unacceptable close contacts between the helix at aa 333–353 of domain II and this active-site loop, indicating that the new conformation was not possible before the cleavage of domain II. The original conformation of the active site in PE is such that 5′-AMP could not be bound in the intact PE without many unacceptable close contacts with the ribose and the phosphate, providing a possible explanation for the observed lack of catalytic activity of intact PE. The observed AMP binding in monomer 2 suggests that one of the events occurring during activation of the PE involves removal of the helix at aa 333–353 of domain II from the vicinity of the cleft, permitting the movement of the aa 458–463 loop, especially Arg-458, away from the center of the substrate-binding cleft.

In monomer 1, the binding site, including the aa 458–463 loop, is quite disordered and is not included in the model, and there is no interpretable difference electron density for the AMP. This loop in monomer 2 is stabilized by interactions with a symmetry-related molecule, and we cannot rule out that the ordering of the loop is due to these interactions. In particular, one of these interactions, an H bond to Arg-609 of adjacent monomer 1, may enhance the binding of AMP. There is no such H-bonding group available in this location around the active site of monomer 1, which might account for the lack of observed AMP in monomer 1.

Comparison with DT. The catalytic domains of PE and DT are among the most homologous of the ADP-transferring toxins [23% sequence identity and 35% conservative substitution (30)]. Both toxins target the same protein, eEF-2, and exhibit similar kinetic constants and inhibitor specificities (30). DT also catalyzes the slow hydrolysis of NAD in the absence of eEF-2 (30) and both toxins contain a cleft with conserved residues (Fig. 3). Experiments that identify putative active-site residues in both toxins give similar results. Complex structures of intact DT and of the isolated catalytic domain have been determined, both with ApUp (21, 23). In ApUp, an inhibitor of DT, the adenosine portion is the same as in NAD, but with a 3′ phosphate vs. the 5′ phosphate as in NAD. Also, because of the pyrophosphate linkage in NAD, the position of the uracil and the nicotinamide can be expected to be different. When we compare the interactions of DT with ApUp and PEIII with AMP and nicotinamide, we observe some similarity in the location of the adenosines (Fig. 3; Table 3). The ribose moieties almost superimpose, while the adenines, although they do not closely superimpose, nevertheless, make similar contacts with the protein. The polypeptide main chain at Gly-454 and Arg-456 in PEIII is H bonded to the adenine in a similar manner to that at Gly-34 and Gln-36 in DT. His-440 also interacts with ribose in a similar way to His-21 in DT. However, not unexpectedly, there are significant differences in the phosphate positions. The 3′ phosphate in ApUp of DT is located in the middle of the cleft, whereas the 5′ phosphate of AMP in PEIII is directed toward the aa 458–463 loop and forms an H bond with Arg-458. However, the position of the 5′ phosphate group in AMP can be readily changed by rotation about the two single bonds (C4—C5 and C5—O5′), and the position of this phosphate could be different when intact NAD is bound.

The nicotinamide is located in the same position in both monomers of domain III. This position differs from the uracil position in DT. In PEIII, the nicotinamide is closer to Glu-553, an essential residue for ADP-ribose transfer, with a distance between the C^{α} of this residue and the closest atom of nicotinamide of 4.67 Å in monomer 2, while, in DT, the distance to the nearest atom of the uracil is 7.44 Å.

Active-Site Residues. The residues involved in binding AMP and nicotinamide in PEIII are all located in the substrate-binding cleft (Fig. 1; Table 3). The results from this structure analysis support previous assignments of the residues that bind NAD (12–14). As proposed (15, 31), H bonds and charge-neutralization interactions are formed between Arg-458 and the phosphate group of AMP. Site-specific substitution with different amino acids indicates that His-21 in DT is important in both NAD binding and transfer of ADP-ribose to eEF-2 (32). The corresponding residue in PT, His-35, has been found to be critical for NAD binding and glycohydrolysis (33). However, data from similar experiments on PE show that, although substitution of the His-440 with Ala, Asn, or Phe reduced the ADP-ribosylation activity to 1/1000th, it did not reduce NAD binding or NAD-glycohydrolase activity (34). In the PEIII structure, His-440 forms a hydrogen bond with the AMP ribose, which is consistent with results from DT and pertussis toxin (32, 33) and with the observed interaction between ApUp and His-21 in the DT structure (21, 23). Thr-442 and Ser-449, which bind to AMP in monomer 2, were not involved in ApUp binding in the DT structure. The nicotinamide ring forms a stacking interaction with Tyr-481 as predicted in ref. 31. The location of Glu-553 in PEIII is consistent with photolabel (35) and site-directed mutagenesis

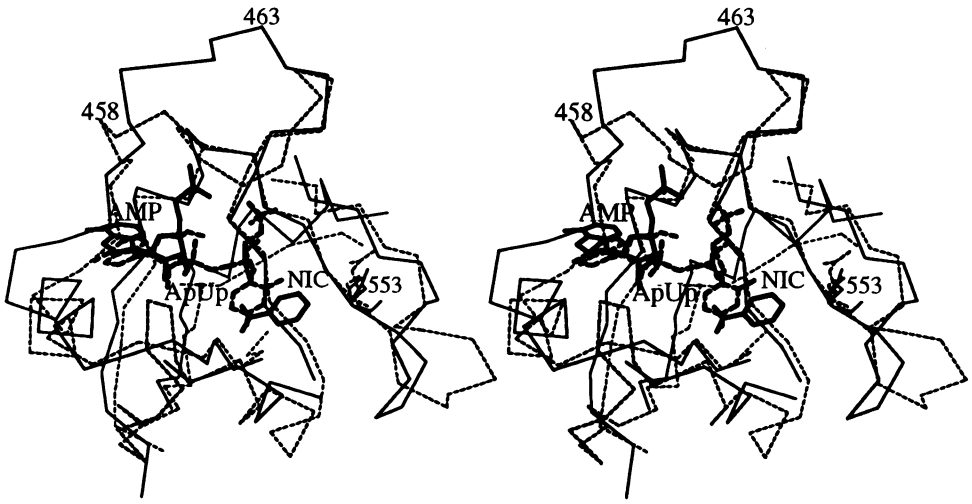

FIG. 3. Stereoview of the active site of the catalytic domain of DT (dashed lines) with bound ApUp (bold, dashed lines) superimposed on monomer 2 of PEIII (solid lines) with AMP (bold, solid lines) and nicotinamide (NIC; bold, solid lines). The figure was drawn by using MOLSCRIPT (29).

experiments (13). The photoaffinity labeling located this residue in the nicotinamide-binding subsite (12); the conservative substitution of Glu-553 by Asp caused substantial losses in both toxicity and ADP-ribosylation activity, without affecting NAD binding (13).

Trp-466 is conserved among ADP-ribosyltransferases, and previous modeling studies (31) suggested that it can be oriented to stack against the nicotinamide or the adenine; we do not observe any interaction with this side chain. The environment of Trp-466 in PEIII reveals a local hydrophobic core which is also found in the DT and PE structure, consisting of Ile-465, Leu-535, Val-527, Ile-542, Leu-537, Ile-555, and Leu-518, suggesting that perhaps this Trp-466 may be more important for conformational stability than for substrate binding.

We have modeled the binding of NAD in the active site of PEIII, placing the NAD in the cleft on the basis of the observed positions of AMP and nicotinamide. The interactions between the enzyme and the AMP and nicotinamide portions of NAD remain unchanged, except that the nicotinamide rotates slightly. The second phosphate and ribose fit the cleft without requiring any conformational change in the main chain. By changing the side-chain torsion angles, the guanidinium group of Arg-467 can be moved into the cleft to form H bonds with the second phosphate. The second ribose stacks against the phenol ring of Tyr-470, another conserved residue (29), located at the bottom of the cleft. Preliminary results from an examination of the complex of domain III with a nonhydrolyzable NAD analog support the general features of this model (unpublished data).

We thank Dr. David McKay for sending us the latest set of coordinates for the intact *Pseudomonas aeruginosa* exotoxin A. We also thank Dr. David Eisenberg for the coordinates of the intact diphtheria toxin and of the isolated catalytic domain.

1. Iglewski, B. H. & Kabat, D. (1975) *Proc. Natl. Acad. Sci. USA* **72,** 2284–2288.
2. Pastan, I., Chaudhary, V. K. & FitzGerald, D. (1992) *Annu. Rev. Biochem.* **61,** 331–354.
3. Kounnas, M. Z., Morris, R. E., Thompson, M. R., FitzGerald, D. J., Strickland, D. K. & Saelinger, C. B. (1992) *J. Biol. Chem.* **267,** 12420–12423.
4. Zdanovsky, A. G., Chiron, M., Pastan, I. & FitzGerald, D. J. (1993) *J. Biol. Chem.* **268,** 21791–21799.
5. Hwang, J., FitzGerald, D., Adhya, S. & Pastan, I. (1987) *Cell* **48,** 129–136.
6. Allured, V. S., Collier, R. J., Carroll, S. F. & McKay, D. B. (1986) *Proc. Natl. Acad. Sci. USA* **83,** 1320–1324.
7. Jinno, Y., Chaudhary, V. K., Kondo, T., Adhya, S., FitzGerald, D. J. & Pastan, I. (1988) *J. Biol. Chem.* **263,** 13203–13207.
8. Siegall, C. B., Chaudhary, V. K., FitzGerald, D. J. & Pastan, I. (1989) *J. Biol. Chem.* **264,** 14256–14261.
9. Chaudhary, V. K., Jinno, Y., FitzGerald, D. J. & Pastan, I. (1990) *Proc. Natl. Acad. Sci. USA* **87,** 308–312.
10. Seetharam, S., Chaudhary, V. K., FitzGerald, D. J. & Pastan, I. (1991) *J. Biol. Chem.* **266,** 17376–17381.
11. Kessler, S. P. & Galloway, D. R. (1992) *J. Biol. Chem.* **267,** 19107–19111.
12. Lukac, M., Pier, G. B. & Collier, R. J. (1988) *Infect. Immun.* **56,** 3095–3098.
13. Douglas, C. M. & Collier, R. J. (1990) *Biochemistry* **29,** 5043–5049.
14. Lukac, M. & Collier, R. J. (1988) *Biochemistry* **27,** 7629–7632.
15. Brandhuber, B., Allured, V. S., Falbel, T. G. & McKay, D. B. (1988) *Proteins* **3,** 146–154.
16. Chung, D. W. & Collier, R. J. (1977) *Infect. Immun.* **16,** 832–841.
17. Lory, S. & Collier, R. J. (1980) *Infect. Immun.* **28,** 494–501.
18. Brinkmann, U. & Pastan, I. (1994) *Biochim. Biophys. Acta* **1198,** 27–45.
19. Pastan, I., Pai, L., Brinkmann, U. & FitzGerald, D. (1995) *Ann. N.Y. Acad. Sci.*, in press.
20. Sixma, T. K., Pronk, S. E., Kalk, K. H., Wartna, E. S., Zanten, B. A. M., Withholt, B. & Hol, W. G. J. (1991) *Nature (London)* **351,** 371–377.
21. Choe, S., Bennett, M. J., Fujii, G., Curmi, P. M. G., Kantardjieff, K. A., Collier, R. J. & Eisenberg, D. (1992) *Nature (London)* **357,** 216–222.
22. Stein, P. E., Boodhoo, A., Armstrong, G. D., Cockle, S. A., Klein, M. H. & Read, R. J. (1994) *Structure* **2,** 45–57.
23. Weiss, M., Blanke, S., Collier, R. J. & Eisenberg, D. (1995) *Biochemistry* **34,** 773–781.
24. Studier, F. & Moffat, B. (1986) *J. Mol. Biol.* **189,** 113–130.
25. Benhar, I., Wang, Q., FitzGerald, D. & Pastan, I. (1994) *J. Biol. Chem.* **269,** 13398–13404.
26. Jancarik, J. & Kim, S. H. (1991) *J. Appl. Crystallogr.* **24,** 409–411.
27. Navaza, J. (1994) *Acta Crystallogr.* **50,** 157–163.
28. Jones, T. A., Zou, J.-Y., Cowan, S. W. & Kjeldgaard, M. (1991) *Acta Crystallogr.* **47,** 110–119.
29. Kraulis, P. (1991) *J. Appl. Crystallogr.* **24,** 946–950.
30. Carroll, S. F. & Collier, R. J. (1988) *Mol. Microbiol.* **2,** 293–296.
31. Domenighini, M., Montecucco, C., Ripka, W. C. & Rappuoli, R. (1991) *Mol. Microbiol.* **5,** 23–31.
32. Blanke, S. R., Huang, K., Wilson, B. A., Papini, E., Covacci, A. & Collier, R. J. (1994) *Biochemistry* **33,** 5155–5161.
33. Antoine, R. & Locht, C. (1994) *J. Biol. Chem.* **269,** 6450–6457.
34. Han, X. Y. & Galloway, D. R. (1995) *J. Biol. Chem.* **270,** 679–684.
35. Carroll, S. F. & Collier, R. J. (1987) *J. Biol. Chem.* **262,** 8707–8711.